PCCP

PAPER

View Article Online
View Journal | View Issue

Cite this: *Phys. Chem. Chem. Phys.*, 2016, **18**, 18507

A DFT study of planar *vs.* corrugated graphene-like carbon nitride (g-C_3N_4) and its role in the catalytic performance of CO_2 conversion†

Luis Miguel Azofra, Douglas R. MacFarlane and Chenghua Sun*

Received 13th April 2016,
Accepted 13th June 2016

DOI: 10.1039/c6cp02453j

www.rsc.org/pccp

Graphene-like carbon nitride (g-C_3N_4), a metal-free 2D material that is of interest as a CO_2 reduction catalyst, is stabilised by corrugation in order to minimise the electronic repulsions experienced by the N lone pairs located in their structural holes. This conformational change not only stabilises the Fermi level in comparison with the totally planar structure, but also increases the potential depth of the π-holes, representing the active sites where the catalytic CO_2 conversion takes place. Finally, as a result of corrugation, our DFT-D3 calculations indicate that the reaction Gibbs free energy for the first H^+/e^- addition decreases by 0.49 eV with respect to the totally planar case, suggesting that corrugation not only involves the material's stabilisation but also enhances the catalytic performance for the selective production of CO/CH_3OH.

Introduction

Since in 1989 Liu and Cohen theoretically predicted the existence of hypothetical covalent solids solely constituted by carbon and nitrogen,[1] extensive and rich literature has emerged in the recent decades concerning the synthesis of the so-called graphene-like carbon nitride (g-C_3N_4) nano-materials.[2] In this regard, g-C_3N_4 nanosheets are 2D sheets which can be synthesised by the pyrolysis of nitrogen-rich precursors such as triazine-based monomers, leading to π-conjugated meshes in which C and N atoms are sp^2-hybridised and polymerically connected *via* tertiary amine groups (see Scheme 1).[3]

Among the many CN-containing allotropes, g-C_3N_4 is the most stable under mild conditions (*i.e.* ambient temperatures and pressures), showing a high thermal stability in air up to 600 °C[4] and being stable in water solution and non-soluble in both acidic and basic solvents.[5] Thus, this high stability of g-C_3N_4 along with many other properties such as its earth-abundance and metal-free composition, easy, inexpensive and large quantity production,[6] the ability to be easily composited with coating materials to increase its the surface area,[7] and its behaviour as a p-type semiconductor (band gap = 2.7 eV, see Scheme 1) make this novel material a promising candidate for the development of applications in heterogeneous catalysis.

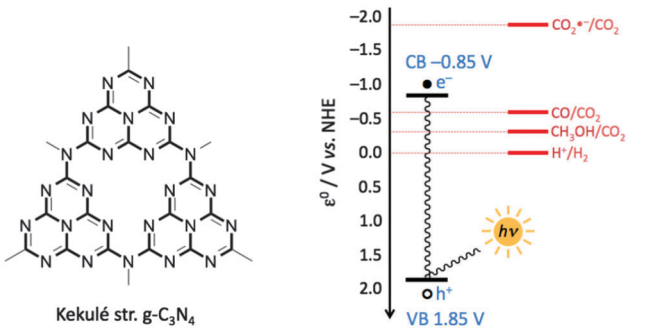

Scheme 1 Kekulé structure representation of g-C_3N_4 (left) and schematic illustration of valence (VB) and conductive (CB) band positions in g-C_3N_4 (at pH = 7) *vs.* normal hydrogen electrode (NHE, right).

In recent years, both experimental[5,8,9] and theoretical[10–13] studies have been published highlighting the ability and describing the mechanisms followed by g-C_3N_4 as a catalyst in H_2 production through water splitting. More recently the ability of this material to capture CO_2 has been demonstrated when functionalised with porous reduced graphene oxide aerogel surfaces.[14] In that sense, the research carried out by Kim and co-workers is of paramount importance since it not only leads to an advancement in the challenging CO_2 capture technology, but also because CO_2 physisorption represents the first step in the CO_2 conversion into hydrocarbon compounds. In this regard, a non-covalent interaction, normally of $O{=}C{=}O_{lp}\cdots M$ nature with M being an electropositive atom, comes into play in order to fix CO_2 on the surface; notwithstanding CO_2 physisorption is usually thermodynamically

ARC Centre of Excellence for Electromaterials Science (ACES), School of Chemistry, Faculty of Science, Monash University, Clayton, VIC 3800, Australia.
E-mail: Chenghua.Sun@monash.edu; Fax: (+61) 3 9905 4597;
Tel: (+61) 3 9902 9916

† Electronic supplementary information (ESI) available: Additional computational details, structures and energies. See DOI: 10.1039/c6cp02453j

non-spontaneous under mild conditions and additional energy/pressure is required to enhance such contact in most of the common materials. Improved strategies have been investigated by Illas and co-workers when interacting CO_2 with cations[15] and novel transition metal carbide materials.[16] Also, Meng *et al.* show that the use of alkali reagents to modify the surface of TiO_2 increases CO_2 adsorption, and also activates the subsequent conversion.[17]

Recently, some efforts have been directed towards the use of g-C_3N_4 as a catalyst that artificially mimics photosynthesis in plants for the CO_2 conversion into hydrocarbon fuels when composited with a series of metal oxides;[18–21] however there is no consensus as to the mechanistic role of each species in the composite. Also, novel strategies by non-metal doping of g-C_3N_4 have demonstrated to enhance the photo-catalytic CO_2 reduction performance,[22,23] and more recently, Du and co-workers have theoretically confirmed important decreases in the rate-determining barriers when supporting single atom Pd/Pt on g-C_3N_4.[24] In any case, these studies elaborate the observations made by Mao *et al.*[25] who experimentally confirmed that g-C_3N_4 based on urea as building block (u-g-C_3N_4) catalyses the CO_2 conversion into CH_3OH and C_2H_5OH with yields of 15.1 and 10.8 μmol after 12 h of VIS-light irradiation, respectively. On the other hand, Dong *et al.*[26] obtained predominantly CO in their CO_2 reduction experiments.

Against this background, it is of crucial importance to unravel the mechanistic aspects of these reactions and understand why and how this novel material works as a CO_2 conversion catalyst. In particular the different conformations (*e.g.* planar *vs.* corrugated) of the 2D material may be very important for determining the activity of the active sites. In short, in the present work, our investigations based on well-resolved density functional theory shed light onto the debate existing about the stability of the planar *vs.* corrugated forms of g-C_3N_4 through the analysis of the conformational landscape and the implication of such differences in the catalytic performance of the CO_2 conversion mechanism.

Computational details

The mechanism for the electrochemical conversion of CO_2 into hydrocarbon compounds catalysed by graphene-like carbon nitride nano-sheets or meshes (g-C_3N_4) has been studied by means of density functional theory (DFT) through the generalized gradient approximation (GGA) with the Perdew–Burke–Ernzerhof (PBE) functional,[27,28] using a plane-wave cut-off energy of 450 eV.[29,30] For those neutral states, no special spin considerations were taken into account, while for radical intermediates, spin-polarised calculations were performed in all models. Concerning the periodic boundary conditions, the Brillouin zone was sampled by 3 × 3 × 1 *k*-points using the Monkhorst–Pack scheme, having tested a larger set of *k*-points for making sure that there were no significant changes in the calculated energies. In order to avoid interactions between periodic images, a vacuum distance of 20 Å was imposed between different layers. At the first stage, optimisation calculations with and without geometrical constraints were done using energy and force convergence limits equal to 10^{-4} eV per atom and 0.05/0.01 eV $Å^{-1}$ for planar and corrugated g-C_3N_4, respectively. With the aim to obtain more accurate values, re-optimisations employing D3 Grimme's method (DFT-D3)[31,32] were carried out in order to include explicit dispersion correction terms to the energy. (Further technical discussion of the methodology can be found in the ESI†.) Also, in order to evaluate the zero point energy (ZPE) as well as the thermal correction terms, additional calculations over the Γ points were carried at the DFT-D3 computational level. Finally, the effect of the water environment was analysed through the modelling of thirteen (13) explicit H_2O molecules interacting on the corrugated g-C_3N_4. For such purposes, optimised structures were used as initial configurations for the *NVT* canonical ensemble (T = 298 K) molecular dynamics (MD) simulation along 2000 steps and 1 fs per step (2 ps in total). (DFT-D2[33] MD, full details in the ESI†). Once equilibrium was reached and checked, re-optimisations at the DFT-D3 level were carried out. All optimisation, single point, and MD calculations have been performed through the facilities provided by the Vienna *Ab Initio* Simulation Package (VASP, version 5.3.5).[34–37]

The analysis of the maxima and minima of the molecular electrostatic potential (MEP) on the 0.001 au electron density iso-surface has been performed using the WFA-SAS program[38] over representative quantum dots (QDs) at the PBE0/6-31+G(d)[39] computational level, having previously optimised and corroborated their condition of minima on the potential energy surface (PES) through the calculation of vibrational frequencies using the Gaussian09 (revision D.01) package.[40]

Finally, the reaction mechanism thermodynamics has been calculated using eqn (1), where n is the number of H^+/e^- pairs transferred and m the number of H_2O molecules released, if applicable. In such context, the chemical potential of the H^+/e^- pair has the half value of the chemical potential of the dihydrogen (H_2) molecule [see eqn (2)][41] under standard conditions of pH = 0, $f(H_2)$ = 101, 325 Pa, and U = 0 V *vs.* standard hydrogen electrode (SHE).

$$\Delta G_R = G(\text{surf}\cdots\text{CO}_{2-m}\text{H}_{n-2m}) + mG(\text{H}_2\text{O}) - G(\text{surf}) - G(\text{CO}_2) - n/2G(\text{H}_2) \quad (1)$$

$$\mu(\text{H}^+/\text{e}^-) = \tfrac{1}{2}\mu(\text{H}_2) \quad (2)$$

Results and discussion

Stabilisation and properties of planar *vs.* corrugated g-C_3N_4

We start with a primary question – what does 'corrugation' mean? We say that a surface is corrugated when ridge or groove defects appear that modify/deform a planar structure. Our DFT-GGA calculations using PBE as a functional and a plane-wave cut-off energy of 450 eV with 3 × 3 × 1 *k*-points (see Computational details below) indicate that corrugated 2 × 2 g-C_3N_4 sheets experience a strong deformation of the planarity, with differences along the *Z*-axis of as much as 2.62 Å (Fig. 1, top). It is noteworthy that corrugation also causes contraction of the lattice parameters, with diminutions of 0.30 Å per unit of tri-*s*-triazine moieties.

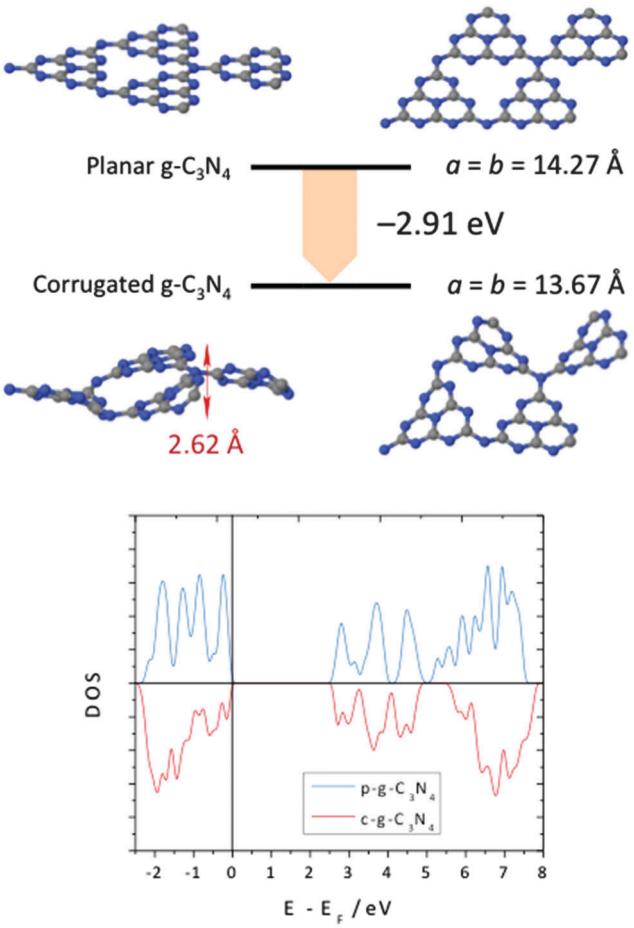

Fig. 1 Optimised structures for planar and corrugated 2 × 2 g-C_3N_4 sheets and their corresponding density of state (DOS) profiles.

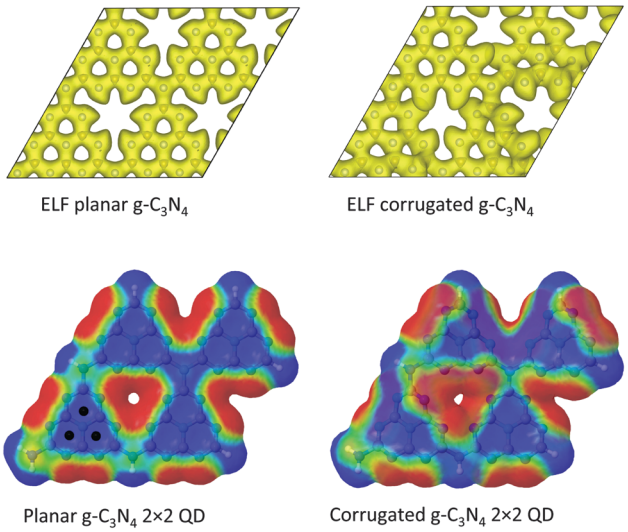

Fig. 2 Electron localization function (ELF) representations and molecular electrostatic potential (MEP) on the 0.001 au electron-density iso-surface for representative g-C_3N_4 quantum dots. Black spheres indicate representative π-holes on the MEP contour (±0.02 au).

Apart from the geometric differences, corrugation in g-C_3N_4 generates energy stabilisation. The enthalpy difference (ΔH) between planar and corrugated 2 × 2 sheets reaches 2.91 eV in favour of the latter, and a similar value is also obtained when comparing larger sets of *k*-points (up to 6 × 6 × 1). For comparative purposes, this energy value is around 50% of the stored energy in the C–C covalent bond of ethane, highlighting the magnitude of such stabilisation. Between the totally planar and most corrugated structures, a set of intermediate distorted minima can be found as a function of deformation, leading to the conclusion that corrugation provides stabilisation that is related to the magnitude of deformation.

Moreover, changes in the electronic structure of the distorted carbon nitride network become evident when the density of states (DOS) is calculated. Our DFT results using the PBE functional show an important diminution at the Fermi level, from −3.55 eV in the planar case to −4.30 eV once corrugation takes place, notwithstanding that results at this computational level underestimate the VB–CB band gap. More accurate single point HSE06[42–44] calculations over the optimised PBE structures indicate band gaps of 2.71 and 2.61 eV for the planar and corrugated cases (at bottom in Fig. 1), respectively, which are in very good agreement with the experimental value of 2.7 eV,[45] which corresponds to the absorption in the blue-VIS area (up to 450 nm).

However, a major question still arises. Which are the factors that lead to energy stabilisation in g-C_3N_4 as a result of corrugation? As suggested by Gracia *et al.*,[46] corrugation intrinsically involves the partial breakage or weakening of π delocalisation over triazine moieties, which would normally be thought of as producing energy destabilisation. However, electron localization function (ELF) analysis can provide insight into why corrugated g-C_3N_4 is thermodynamically more favoured than the planar isomer, as shown at the top in Fig. 2. By condensation of the tri-*s*-triazine monomers, g-C_3N_4 displays a set of structural holes, towards which the N lone pairs (N_{lp}) point (see structures in Fig. 1). Such N_{lp} experience larger electronic repulsions in the planar case because each points towards its neighbouring N_{lp}. As shown in Fig. 2 (top) once g-C_3N_4 corrugates, the sinusoidal-like shape minimises such repulsions. This effect occurs with φ_{NCCN} dihedral angles, in which N and C are sp^2-hybridised atoms, changing from *cis*(0°) to a half-*gauche* (≈30°) conformations.

Catalytic performance for the CO_2 conversion mechanism

CO_2 conversion technology has a goal of the production of hydrocarbon compounds from CO_2, producing 'green fuels' with a zero-balance of greenhouse gas emissions. In recent years, important advances have been made in the description of metal-based catalysts for the photo-electrochemical conversion of CO_2 into hydrocarbon compounds.[47–50] However, g-C_3N_4 is emerging as a promising alternative not only due to its metal-free composition, but also due to its inherent band gap as a semiconductor material (2.7 eV)[45] and much more remarkably, due to its easy, inexpensive and potential for large-scale production.[6] Recent investigations have demonstrated the ability of g-C_3N_4 as a catalyst for CO_2 conversion, notwithstanding that there are some controversies concerning the selectivity of this

material towards the production of CO or CH_3OH/C_2H_5OH compounds,[25,26] in addition to the still poor yields obtained.

Molecular electrostatic potential (MEP) calculations on the 0.001 au electron density iso-surface for representative 2×2 g-C_3N_4 quantum dots (Fig. 2 bottom) show that corrugation enhances the depth of the π-holes associated with the π-conjugated rings. $V_{s,max}$ increases from 1.44 to 1.61 eV, values that suggest that corrugation should improve the catalytic performance for CO_2 conversion. Such a link between π-hole depth and catalysis has been suggested for other 2D materials.[51] Thus, and as indicated in Fig. 3a, planar g-C_3N_4 is hypothesised to be selective towards the formation of methanol when converting CO_2, because the reaction path follows the formaldehyde route after CO formation. At the beginning, CO_2 physisorption on pure planar g-C_3N_4 displays a non-spontaneous Gibbs free reaction energy at 298 K (ΔG^{298}, hereafter simply referred as reaction energy) of 0.41 eV, in agreement with the aforementioned experimental evidence.[25] More significantly, the first hydrogenation step, consisting of the gain of one H^+/e^- pair to reach HOCO•, displays a reaction energy amounting to 1.64 eV. This profile indicates that g-C_3N_4 exhibits a classical behaviour as a CO_2 conversion catalyst, since the first hydrogenation step is thought to be the limiting step of the whole reaction.[52]

Once HOCO• is obtained, the thermodynamic profile indicates that, in all cases, the formation of neutral products such as CO (with the release of one H_2O molecule), H_2CO, and CH_3OH along the second, fourth, and sixth steps, respectively, is characterised by the release of energy. On the contrary, the formation of radicals connecting such hydrocarbon compounds demand the input of energy, so that the formation of

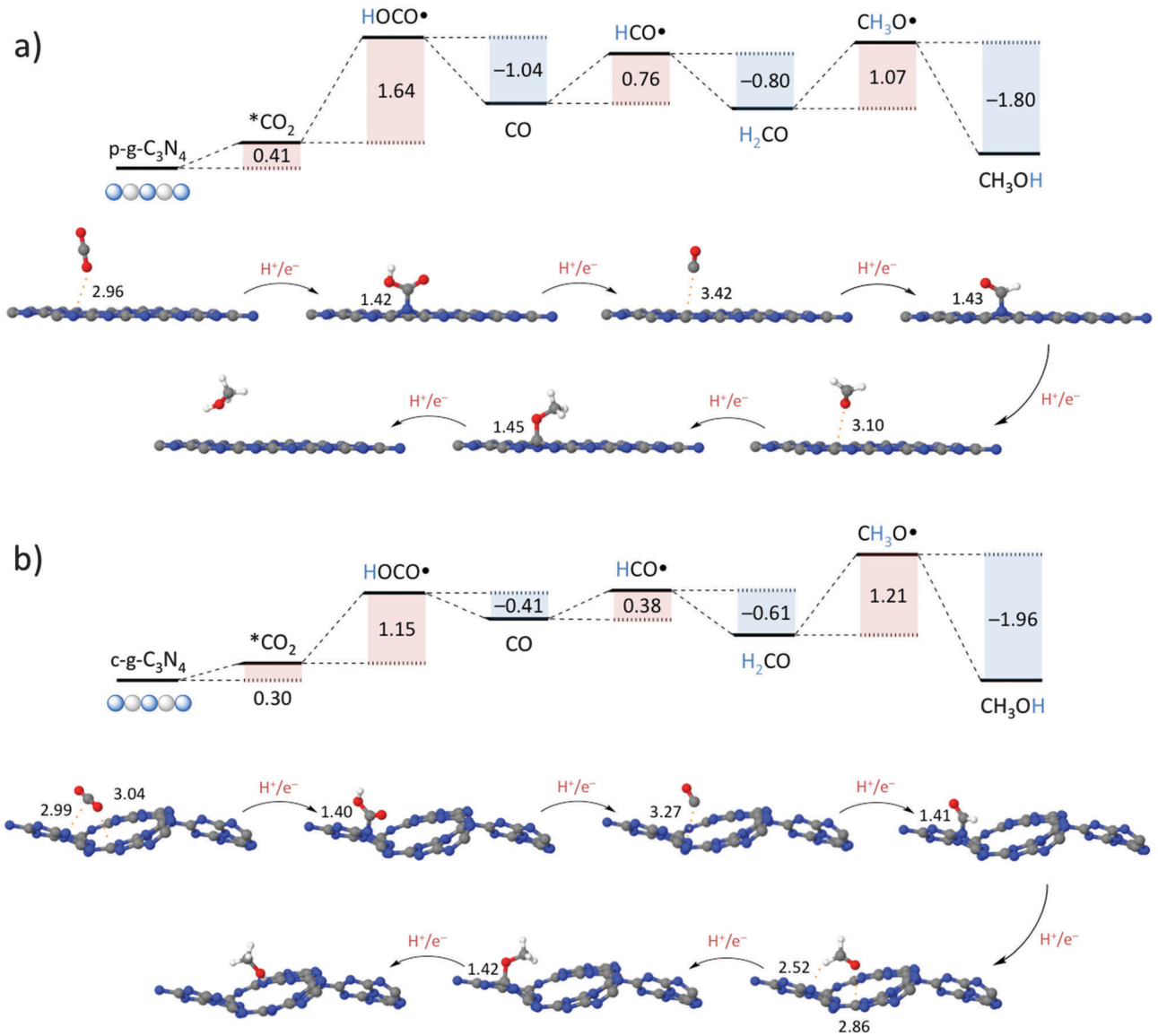

Fig. 3 Gibbs free energy diagram (thermodynamics, in eV) and structures corresponding to the reaction path followed by the CO_2 conversion mechanism into CO, H_2CO, and CH_3OH catalysed by: (a) planar; and (b) corrugated g-C_3N_4 *vs.* SHE, calculated at the DFT-D3 computational level. Selected distances are shown in Å. Chemisorbed (bound) species are indicated by full bonds, while physisorbed species are indicated by dashed bonds.

the radicals $HCO^{\bullet}$ and $CH_3O^{\bullet}$ is a non-spontaneous process requiring an energy input of 0.76 and 1.07 eV, respectively. It deserves to be mentioned that the radical formation implies the electrostatic interaction of these species with the mesh through the π-holes located over the π-conjugated rings. However, while $HOCO^{\bullet}$ and $HCO^{\bullet}$ interact *via* their C moiety with the N atom of the mesh, DFT-D3 predicts that no O–N bond formation occurs in the $H_2CO/CH_3O^{\bullet}$ step. In this particular case, the chemisorption of the radical $CH_3O^{\bullet}$ species takes place through a C moiety from the network.

Impressive behaviour can be seen when the mechanistic DFT-D3 analysis is applied to the corrugated g-C_3N_4 as a catalyst (Fig. 3b). First of all, both the CO_2 fixation on the surface and the first hydrogenation steps show a decrease in energy by 0.11 and 0.49 eV, respectively, compared to the planar case (*i.e.* demanding 0.30 and 1.15 eV, respectively). This observation is in agreement with the increased depth of π-holes, as previously discussed, and highlights the role of corrugation in the enhanced catalytic performance of CO_2 conversion. In this regard, the effect of corrugation is also present in the third H^+/e^- pair gain, once the $HCO^{\bullet}$ intermediate species is formed, in which the energy requirement decreases from 0.76 to 0.38 eV. However, and on the contrary, the O-philicity of the surface seems to be less significant, since the chemisorption of the $CH_3O^{\bullet}$ radical in the fifth step becomes a slightly more non-spontaneous process, and hence becomes the new limiting step of the whole reaction (1.07 *vs.* 1.21 eV for the planar and corrugated meshes). Furthermore, our investigations on alternative routes for the CO_2 conversion mechanism suggest that g-C_3N_4 is not selective towards the formation of the $OCHO^{\bullet}$ species during the first hydrogenation step, and at the same time, the $COH^{\bullet}$ and $H_2COH^{\bullet}$ radicals during the third and fifth H^+/e^- gains are less stable than the respective $HCO^{\bullet}$ and $CH_3O^{\bullet}$ intermediate species, or in other words, implying that the paths respected from these species are thermodynamically dismissed in favour to the ones following the reaction path described at Fig. 3.

From a technical point of view, the explicit inclusion of dispersion using D3 Grimme's method is established as fundamentally necessary for a good theoretical description of the process. In this sense, solute-material distances in neutral and reaction energies in radical species are over- and under-estimated, respectively, when dispersion is not taken into account during optimisation. Using the first and second $HOCO^{\bullet}$ and CO reduced species catalysed by corrugated g-C_3N_4 for instance, the reaction energy varies from 1.58 to 1.15 eV for $HOCO^{\bullet}$ and the C···N distance differs from 3.41 to 3.27 Å for CO. These significant divergences let us to conclude that in addition to electrostatics as the main driving force for the catalysis of CO_2 conversion, a certain dose of dispersion also becomes important.

The role of the H_2O environment

Among the most significant limitations in the modelling of CO_2 conversion mechanisms, the absence of explicit dispersion treatments usually leads to DFT artefacts that provide overvalued energy estimations. In this regard and as has been mentioned in this work, when no dispersion corrections are taken into account in g-C_3N_4, it leads to relative theoretical errors of almost 400 mV – an admittedly large difference, which certainly indicates a deficit in the quantitative prediction. Moreover, the effect of the environment might also play an important role in the catalytic mechanism, thus an explicit evaluation of this is highly desirable. In this regard and in order to provide some results to improve the lack of information on this topic, the CO_2 conversion mechanism catalysed by corrugated g-C_3N_4 has been studied (Fig. 4) in the presence of 13 explicit H_2O molecules, producing an important benchmark with respect to when the aqueous medium is not taken into account. In this regard, the selection of 13 explicit H_2O molecules has been the result of a thorough study in which different *m* numbers of explicit H_2O molecules were tested. Among the variety of results, this so-called '13 H_2O model' ensures: (i) a clear and better description of the events occurring at the 'nano' size scale (*e.g.* hydrophobic/philic interactions with non-polar CO_2 and polar HOCO states, respectively); (ii) enough H_2O molecules to provide a model with both the interactions with the adsorbates and the presence of H_2O molecules on the rest of the surface material; and (iii) ensuring a full mono-layer in which explicit H_2O molecules present reliable H-bonds that connect one to each other. (For such purposes, 2 ps of *NVT* MD at T = 298 K was carried out for each state prior DFT-D3 re-optimisations).

Despite the fact that trends and qualitative results are similar, the presence of explicit H_2O molecules reveals some divergences. On the one hand, the CO_2 physisorption step exhibits a more positive energy, from 0.30 to 0.92 eV. As a consequence of the low solubility of CO_2 in water, the explicit H_2O molecules are placed far from the solute, demonstrated by a conformational landscape where CO_2 clearly shows hydrophobic repulsions with the H_2O molecules. On the other, and contrary to what it is observed in the $*CO_2$ step, the first H^+/e^- pair gain that leads to the radical $HOCO^{\bullet}$ formation, decrease its Gibbs free reaction energy to 0.99 eV (*vs.* 1.15 eV when no explicit H_2O molecules are used in the model), as a result of stabilisation by H-bonds between the H_2O molecules from the environment and this polar $HOCO^{\bullet}$ species. In this regard, the minimum for this state reveals that the H moiety from OCO–$H^{\bullet}$ is partially ceded to the immediately neighbouring H_2O molecule, with R(OH) distances equal to 1.33 and 1.11 Å, respectively.

When corrugation takes place in g-C_3N_4, the sixth $CH_3O^{\bullet}$ formation step becomes the new limiting step of the whole reaction; the explicit presence of H_2O molecules intensifies this effect, increasing the minimum energy input from 1.21 to 1.59 eV. Beyond the weak H-bonds that occur between H_2O and the O atom (poor H-bond acceptor moiety) of $CH_3O^{\bullet}$, our DFT-D3 calculations also reveal strong repulsions between the water environment and the hydrophobic CH_3 part. This explains not only this increase in the reaction energy, but also the root of the divergences between the experimental tests carried out by Mao *et al.*[25] and Dong and co-workers,[26] since this rate-limiting step may cause earlier products, such as CO, to be the main products at lower over-potentials.

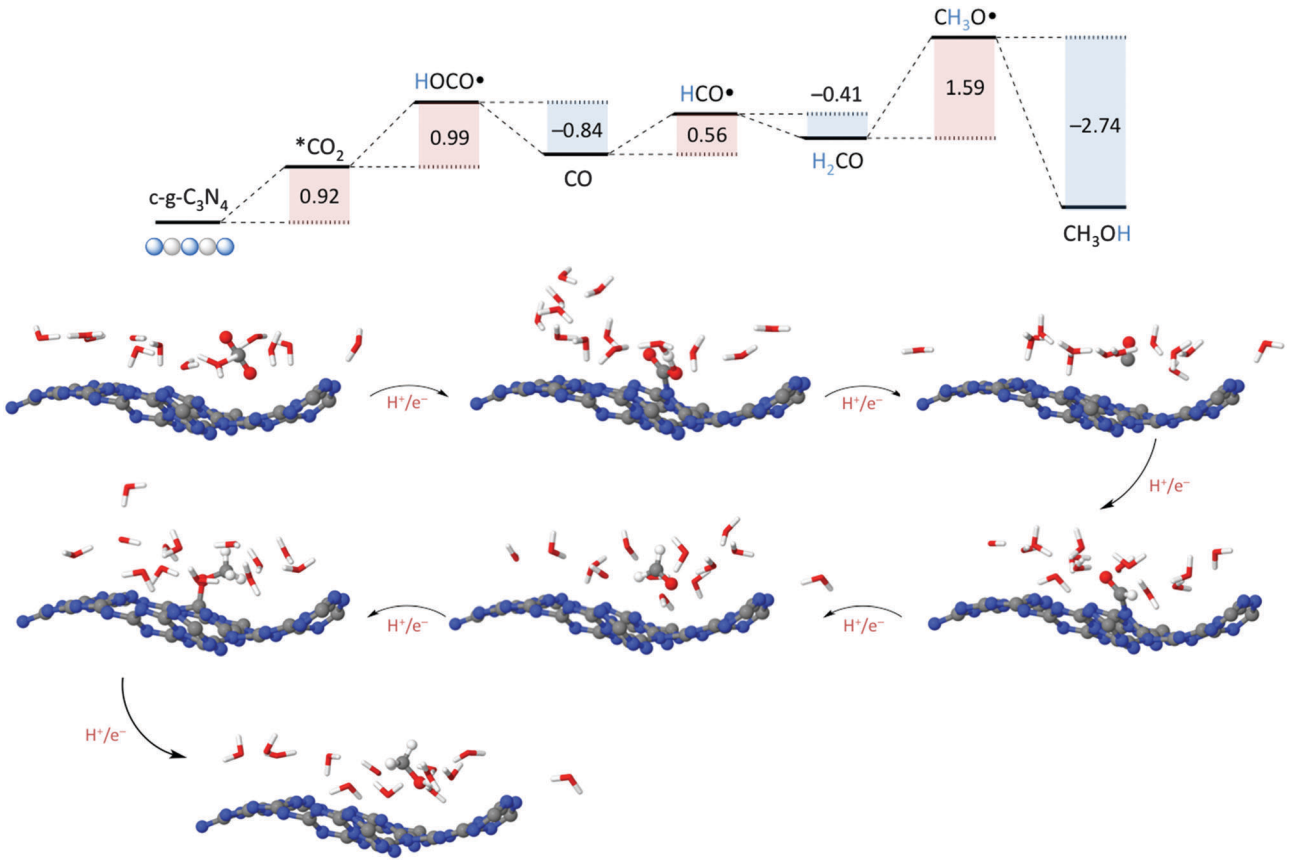

Fig. 4 Gibbs free energy diagram (thermodynamics, in eV) and structures corresponding to the reaction path followed by the CO_2 conversion mechanism into CO, H_2CO, and CH_3OH catalysed by corrugated g-C_3N_4 in the presence of 13 explicit H_2O molecules *vs.* SHE, calculated at the DFT-D3 computational level. Optimised structures after 2 ps DFT-D2 *NVT* MD simulation at T = 298 K.

Conclusions

In summary, our DFT investigations of tri-*s*-triazine based 2×2 graphene-like carbon nitride (g-C_3N_4) indicate that the effect of corrugation involves stabilisation in the carbon nitride mesh and that this is also directly proportional to the magnitude of deformation. In this regard, ΔH between planar and corrugated g-C_3N_4 reaches 2.91 eV in favour of corrugation, a conformational preference acquired by this material in order to minimise the electronic repulsions experienced by the N lone pairs located in their structural holes. Corrugation also enhances the depth of π-holes, which appears to be directly related to the catalytic performance in the CO_2 reduction mechanism. In this regard, while the first hydrogenation transfer to reach HOCO• requires a ΔG^{298} equal to 1.64 eV in planar g-C_3N_4, this value decreases to 1.15 eV when corrugation takes place. The planar mesh requires a higher over-potential in the first reduction step, but as this first step is the rate-limiting step, the reaction then rapidly continues to CH_3OH as the main product. On the contrary in the case of corrugation, the rate-limiting step becomes the sixth step and this may cause earlier products such as CO to be the main products at lower over-potentials. This effect is enhanced when modelling includes 13 explicit H_2O molecules, indicating an increase in reaction energy for the CO_2 physisorption step, but more remarkably, increasing the reaction energy for the CH_3O• formation by up to 1.59 eV. This increase in the sixth step means that it becomes the new limiting step that contrasts with an important concomitant decrease of the first hydrogenation step, which demands only 0.99 eV as a result of stabilisations by H-bonds between the H_2O molecules and the polar HOCO• species. As a general characteristic of the CO_2 conversion mechanism catalysed by g-C_3N_4, our DFT-D3 results hypothesise positive reaction energies (non-spontaneous thermodynamics) when CO_2 is fixed on the surface and when radical formation results from an odd number of H^+/e^- pairs gain, while the release of CO, H_2CO, and CH_3OH compounds (even number of H^+/e^- pairs gain) implies negative reaction energies (spontaneous thermodynamics).

Finally, our work explains for the first time the CO_2 conversion mechanism followed by g-C_3N_4 and provides a series of useful tools for the computer-aided molecular design of future g-C_3N_4 materials/catalysts.

Acknowledgements

The authors acknowledge the Australian Research Council (ARC) for its support through the Australian Centre for

Electromaterials Science (ACES), Discovery Project (DP130100268, CS), Future Fellowship (FT130100076, CS) and Australian Laureate Fellow (DRM) schemes. The National Computational Infrastructure (NCI) is also acknowledged for providing the computational resources. Special thanks are given to Prof. Yong-Hyun Kim's and Prof. Sang Ouk Kim's Groups for providing additional supporting information in relation to their work recently published in ref. 14.

Notes and references

1 A. Y. Liu and M. L. Cohen, *Science*, 1989, **245**, 841–842.
2 (*a*) E. G. Gillan, *Chem. Mater.*, 2000, **12**, 3906–3912; (*b*) V. N. Khabashesku, J. L. Zimmerman and J. L. Margrave, *Chem. Mater.*, 2000, **12**, 3264–3270; (*c*) J. L. Zimmerman, R. Williams, V. N. Khabashesku and J. L. Margrave, *Nano Lett.*, 2001, **1**, 731–734; (*d*) D. R. Miller, J. Wang and E. G. Gillan, *J. Mater. Chem.*, 2002, **12**, 2463–2469; (*e*) G. Algara-Siller, N. Severin, S. Y. Chong, T. Björkman, R. G. Palgrave, A. Laybourn, M. Antonietti, Y. Z. Khimyak, A. V. Krasheninnikov, J. P. Rabe, U. Kaiser, A. I. Cooper, A. Thomas and M. J. Bojdys, *Angew. Chem., Int. Ed.*, 2014, **53**, 7450–7455.
3 Y. Zheng, J. Liu, J. Liang, M. Jaroniec and S. Z. Qiao, *Energy Environ. Sci.*, 2012, **5**, 6717–6731.
4 J. Zhu, Y. Wei, W. Chen, Z. Zhao and A. Thomas, *Chem. Commun.*, 2010, **46**, 6965–6967.
5 X. Wang, K. Maeda, A. Thomas, K. Takanabe, G. Xin, J. M. Carlsson, K. Domen and M. Antonietti, *Nat. Mater.*, 2009, **8**, 76–80.
6 Y. Zhao, Z. Liu, W. Chu, L. Song, Z. Zhang, D. Yu, Y. Tian, S. Xie and L. Sun, *Adv. Mater.*, 2008, **20**, 1777–1781.
7 J. Zhu, P. Xiao, H. Li and S. A. C. Carabineiro, *ACS Appl. Mater. Interfaces*, 2014, **6**, 16449–16465.
8 K. Maeda, X. Wang, Y. Nishihara, D. Lu, M. Antonietti and K. Domen, *J. Phys. Chem. C*, 2009, **113**, 4940–4947.
9 S. Martha, A. Nashim and K. M. Parida, *J. Mater. Chem. A*, 2013, **1**, 7816–7824.
10 C. Butchosa, P. Guiglion and M. A. Zwijnenburg, *J. Phys. Chem. C*, 2014, **118**, 24833–24842.
11 K. Srinivasu, B. Modak and S. K. Ghosh, *J. Phys. Chem. C*, 2014, **118**, 26479–26484.
12 J. Wirth, R. Neumann, M. Antonietti and P. Saalfrank, *Phys. Chem. Chem. Phys.*, 2014, **16**, 15917–15926.
13 G. Gao, Y. Jiao, F. Ma, Y. Jiao, E. Waclawik and A. Du, *J. Catal.*, 2015, **332**, 149–155.
14 Y. Oh, V.-D. Le, U. N. Maiti, J. O. Hwang, W. J. Park, J. Lim, K. E. Lee, Y.-S. Bae, Y.-H. Kim and S. O. Kim, *ACS Nano*, 2015, **9**, 9148–9157.
15 F. Viñes, A. Borodin, O. Höfft, V. Kempter and F. Illas, *Phys. Chem. Chem. Phys.*, 2005, **7**, 3866–3873.
16 C. Kunkel, F. Viñes and F. Illas, *Energy Environ. Sci.*, 2016, **9**, 141–144.
17 X. Meng, S. Ouyang, T. Kako, P. Li, Q. Yu, T. Wang and J. Ye, *Chem. Commun.*, 2014, **50**, 11517–11519.
18 Y. He, Y. Wang, L. Zhang, B. Teng and M. Fan, *Appl. Catal., B*, 2015, **168–169**, 1–8.
19 Y. He, L. Zhang, B. Teng and M. Fan, *Environ. Sci. Technol.*, 2015, **49**, 649–656.
20 H. Shi, C. Zhang, C. Zhou and G. Chen, *RSC Adv.*, 2015, **5**, 93615–93622.
21 W. Yu, D. Xu and T. Peng, *J. Mater. Chem. A*, 2015, **3**, 19936–19947.
22 X. Ma, Y. Lv, J. Xu, Y. Liu, R. Zhang and Y. Zhu, *J. Phys. Chem. C*, 2012, **116**, 23485–23493.
23 K. Wang, Q. Li, B. Liu, B. Cheng, W. Ho and J. Yu, *Appl. Catal., B*, 2015, **176–177**, 44–52.
24 G. Gao, Y. Jiao, E. R. Waclawik and A. Du, *J. Am. Chem. Soc.*, 2016, **138**, 6292–6297.
25 J. Mao, T. Peng, X. Zhang, K. Li, L. Ye and L. Zan, *Catal.: Sci. Technol.*, 2013, **3**, 1253–1260.
26 G. Dong and L. Zhang, *J. Mater. Chem.*, 2012, **22**, 1160–1166.
27 J. P. Perdew, K. Burke and M. Ernzerhof, *Phys. Rev. Lett.*, 1996, **77**, 3865–3868.
28 J. P. Perdew, K. Burke and M. Ernzerhof, *Phys. Rev. Lett.*, 1997, **78**, 1396.
29 P. E. Blöchl, *Phys. Rev. B: Condens. Matter Mater. Phys.*, 1994, **50**, 17953–17979.
30 G. Kresse and D. Joubert, *Phys. Rev. B: Condens. Matter Mater. Phys.*, 1999, **59**, 1758–1775.
31 S. Grimme, J. Antony, S. Ehrlich and H. Krieg, *J. Chem. Phys.*, 2010, **132**, 154104.
32 S. Grimme, S. Ehrlich and L. Goerigk, *J. Comput. Chem.*, 2011, **32**, 1456–1465.
33 J. Harl, L. Schimka and G. Kresse, *Phys. Rev. B: Condens. Matter Mater. Phys.*, 2010, **81**, 115126.
34 G. Kresse and J. Hafner, *Phys. Rev. B: Condens. Matter Mater. Phys.*, 1993, **47**, 558–561.
35 G. Kresse and J. Hafner, *Phys. Rev. B: Condens. Matter Mater. Phys.*, 1994, **49**, 14251–14269.
36 G. Kresse and J. Furthmüller, *Comput. Mater. Sci.*, 1996, **6**, 15–50.
37 G. Kresse and J. Furthmüller, *Phys. Rev. B: Condens. Matter Mater. Phys.*, 1996, **54**, 11169–11186.
38 F. Bulat, A. Toro-Labbé, T. Brinck, J. Murray and P. Politzer, *J. Mol. Model.*, 2010, **16**, 1679–1691.
39 M. J. Frisch, J. A. Pople and J. S. Binkley, *J. Chem. Phys.*, 1984, **80**, 3265–3269.
40 M. J. Frisch, G. W. Trucks, H. B. Schlegel, G. E. Scuseria, M. A. Robb, J. R. Cheeseman, G. Scalmani, V. Barone, B. Mennucci, G. A. Petersson, H. Nakatsuji, M. Caricato, X. Li, H. P. Hratchian, A. F. Izmaylov, J. Bloino, G. Zheng, J. L. Sonnenberg, M. Hada, M. Ehara, K. Toyota, R. Fukuda, J. Hasegawa, M. Ishida, T. Nakajima, Y. Honda, O. Kitao, H. Nakai, T. Vreven, J. A. Montgomery Jr., J. E. Peralta, F. Ogliaro, M. Bearpark, J. J. Heyd, E. Brothers, K. N. Kudin, V. N. Staroverov, R. Kobayashi, J. Normand, K. Raghavachari, A. Rendell, J. C. Burant, S. S. Iyengar, J. Tomasi, M. Cossi, N. Rega, N. J. Millam, M. Klene, J. E. Knox, J. B. Cross, V. Bakken, C. Adamo, J. Jaramillo, R. Gomperts, R. E. Stratmann, O. Yazyev, A. J. Austin, R. Cammi, C. Pomelli, J. W. Ochterski, R. L. Martin, K. Morokuma, V. G. Zakrzewski, G. A. Voth, P. Salvador,

J. J. Dannenberg, S. Dapprich, A. D. Daniels, Ö. Farkas, J. B. Foresman, J. V. Ortiz, J. Cioslowski and D. J. Fox, *Gaussian09 (revision D.01)*, Gaussian, Inc., Wallingford CT, USA, 2009.

41 A. A. Peterson, F. Abild-Pedersen, F. Studt, J. Rossmeisl and J. K. Nørskov, *Energy Environ. Sci.*, 2010, **3**, 1311–1315.

42 J. Heyd, G. E. Scuseria and M. Ernzerhof, *J. Chem. Phys.*, 2003, **118**, 8207–8215.

43 J. Heyd and G. E. Scuseria, *J. Chem. Phys.*, 2004, **121**, 1187–1192.

44 J. Heyd, G. E. Scuseria and M. Ernzerhof, *J. Chem. Phys.*, 2006, **124**, 219906.

45 F. Su, S. C. Mathew, G. Lipner, X. Fu, M. Antonietti, S. Blechert and X. Wang, *J. Am. Chem. Soc.*, 2010, **132**, 16299–16301.

46 J. Gracia and P. Kroll, *J. Mater. Chem.*, 2009, **19**, 3013–3019.

47 A. A. Peterson, F. Abild-Pedersen, F. Studt, J. Rossmeisl and J. K. Nørskov, *Energy Environ. Sci.*, 2010, **3**, 1311–1315.

48 A. A. Peterson and J. K. Nørskov, *J. Phys. Chem. Lett.*, 2012, **3**, 251–258.

49 M. Behrens, F. Studt, I. Kasatkin, S. Kühl, M. Hävecker, F. Abild-Pedersen, S. Zander, F. Girgsdies, P. Kurr, B.-L. Kniep, M. Tovar, R. W. Fischer, J. K. Nørskov and R. Schlögl, *Science*, 2012, **336**, 893–897.

50 H. Li, X. Zhang and D. R. MacFarlane, *Adv. Energy Mater.*, 2015, **5**, 1401077.

51 L. M. Azofra, D. R. MacFarlane and C. Sun, *Chem. Commun.*, 2016, **52**, 3548–3551.

52 W. H. Koppenol and D. J. Rush, *J. Phys. Chem.*, 1987, **91**, 4429–4430.

